



Dielectric, impedance and modulus spectroscopy of BaBi₂Nb₂O₉

Sunanda K. Patri¹ · P. L. Deepti¹ · R. N. P. Choudhary² · B. Behera³

Received: 27 February 2017 / Accepted: 29 March 2018 / Published online: 12 April 2018
© Springer Science+Business Media, LLC, part of Springer Nature 2018

Abstract

Barium Bismuth Niobate (BaBi₂Nb₂O₉) has been synthesized by solid state reaction method. The X-ray diffraction study confirms the formation of compound. Morphological analysis has been carried out from the scanning electron microscopy images and the elemental analysis from the energy dispersive spectroscopy profiles. Investigation of dielectric and ferroelectric properties of the sample was done by varying the temperature from 25 °C - 500 °C in a frequency range of 1 kHz- 1 MHz. At 100 kHz, the phase transition was observed at 214.02°C. Further, this ferroelectric bi-layered perovskite exhibits an interesting relaxor behavior with a strong dispersion of the dielectric permittivity. A detailed study on the impedance spectroscopy over a wide range of temperature and frequency exhibits the contribution of grain and grain boundary on different electrical parameters. From modulus spectroscopy, the presence of non-Debye type of relaxation in the material has been manifested. The complex modulus plots support the negative temperature coefficient of resistance (NTCR) type behavior of the material.

Keywords BaBi₂Nb₂O₉ · Solid state reaction · Relaxor ferroelectrics · Dielectric permittivity

1 Introduction

After the discovery of bismuth layered-structure ferroelectrics (BLSF) by Aurivillius in 1949, many bismuth layered structures have been reported and were investigated. In recent years, BLSF have received much attention as they have multiple applications owing to their exceptional dielectric properties. These materials exhibit potential applications in non-volatile random access memory (NVRAM) for their large remanent polarization P_r , low coercive field E_c and high Curie temperature T_c [1, 2]. The fatigue resistance against polarization switching has become the most interesting aspect of these materials.

The general formula of BLSF compounds is given by $\text{Bi}_2\text{A}_{n-1}\text{B}_n\text{O}_{3n+3}$, with a regular intergrowth of $(\text{Bi}_2\text{O}_2)^{2+}$ layers and perovskite like $(\text{A}_{n-1}\text{B}_n\text{O}_{3n+1})^{2-}$ slabs, where n

represents the number of perovskite layers sandwiched between the bismuth oxide layers. In the above expression $A = \text{Ca, Sr, Pb, Ba}$ etc. is in 12-fold co-ordination, $B = \text{V, Ta, Nb}$ etc., is in six-fold co-ordination. The spontaneous polarization in these types of materials is due to the displacement of B-cations as well as tilting of the BO_6 octahedra. The $(\text{Bi}_2\text{O}_2)^{2+}$ layers act as the insulating paraelectric layers and control the electrical response like electrical conductivity while the ferroelectricity arises predominantly in perovskite blocks. Most of the compounds in this family are well studied and are found to be normal ferroelectrics like $\text{SrBi}_2\text{Nb}_2\text{O}_9$, $\text{SrBi}_2\text{Ta}_2\text{O}_9$ etc. [3, 4]. However, in this respective series, there are many relaxor ferroelectrics such as $\text{BaBi}_2\text{Nb}_2\text{O}_9$, $\text{BaBi}_2\text{Ta}_2\text{O}_9$ [5, 6] show interesting phenomena. The relaxor ferroelectric $\text{BaBi}_2\text{Nb}_2\text{O}_9$ is a member of BLSF with $n = 2$. Relaxor ferroelectrics have been a subject of intense research for their high dielectric constant and giant electrostriction properties [7]. The relaxor behavior is characterized by a strong frequency dependent broadened dielectric peak [8]. It has been claimed that the relaxor behavior is related to the microscopic distortion in a macroscopic tetragonal lattice [9] and to the positional disorder between Bi^{3+} and A^{2+} cations [10, 11]. The presence of cationic disorder was originally proposed by Smolenski [12] in $\text{BaBi}_2\text{Ta}_2\text{O}_9$ and recently confirmed via neutron diffraction studies. In this paper, we report the structure-property correlation of $\text{BaBi}_2\text{Nb}_2\text{O}_9$.

✉ Sunanda K. Patri
sunanda.patri@gmail.com

¹ Department of Physics, Veer Surendra Sai University of Technology, Burla, Sambalpur Odisha-768018, India

² Department of Physics, Institute of Technical Education and Research, Bhubaneswar, India

³ Department of Physics, Sambalpur University, Jyoti Vihar, Sambalpur Odisha-768019, India

2 Experimental

Barium bismuth niobate, $\text{BaBi}_2\text{Nb}_2\text{O}_9$ (BBN) has been prepared by solid state reaction technique. Stoichiometric amounts of reagent grade bismuth oxide (Bi_2O_3 CDH, 99%), niobium oxide (Nb_2O_5 Loba, 99%) and barium carbonate (BaCO_3 CDH, 99%) were weighed and dry grinded for 1 h 30 min followed by wet grinding with methanol for 2 h. An extra amount (2%) of Bi_2O_3 was added to the starting mixture to compensate the bismuth loss at high temperature. The powder mixture was dried and calcined at 900 °C for 4 h. The calcined powder was grounded and cold pressed into small cylindrical pellets of about 10 mm diameter, and 1–5 mm thickness under an isostatic pressure of $4 \times 10^6 \text{ Nm}^{-2}$ with polyvinyl alcohol (PVA) as the binder. High densification of the pellets was obtained after sintering at 1100 °C for 4 h. The confirmation of formation of phase and the crystalline structure of the calcined powders were determined by using X-ray diffraction (XRD) technique at room temperature with a powder diffractometer (ULTIMA IV Model - Rigaku, Japan) using CuK_α radiation ($\lambda = 1.5405 \text{ \AA}$) in a wide range of Bragg's angles 2θ ($20^\circ \leq \theta \leq 80^\circ$) with a scanning rate of $4^\circ/\text{min}$. Microstructural study of the sample has been done by using HITACHI, SU3500, Scanning electron microscope (SEM). For dielectric study, both the surfaces of the sintered pellets were polished to get uniform parallel surface and the electroding is done by applying silver paste at both the surfaces. Dielectric properties were measured by a N4L, PSM1735 LCR meter in the frequency range from 1 kHz to 1 MHz with the temperature varying from room temperature to 500 °C.

3 Results and discussion

3.1 Structural and microstructural studies

The $\text{BaBi}_2\text{Nb}_2\text{O}_9$ compound calcined at 900 °C were characterized by using XRD for the confirmation of purity of phase which is shown in Fig. 1. Based on the XRD profiles, the diffraction pattern observed for the sample was matched with the reported values of tetragonal $\text{BaBi}_2\text{Nb}_2\text{O}_9$ (JCPDS: 00–040–0355). The crystallite size (D) was calculated by Scherrer's equation,

$$d = \frac{k\lambda}{\beta \cos\theta}$$

where, k = shape factor (0.94), β = full width half maxima (FWHM), θ = the Bragg's angle, λ = wavelength of X-ray. The calculated lattice parameters calculated by X'Pert High score software are $a = 3.9360 \text{ \AA}$, $b = 3.9360 \text{ \AA}$ and $c = 25.6130 \text{ \AA}$ and $\alpha = \beta = \gamma = 90^\circ$, which belongs to space group 139:14/mmm and volume (V) = 396.80 \AA^3 . Ismunandar et al.

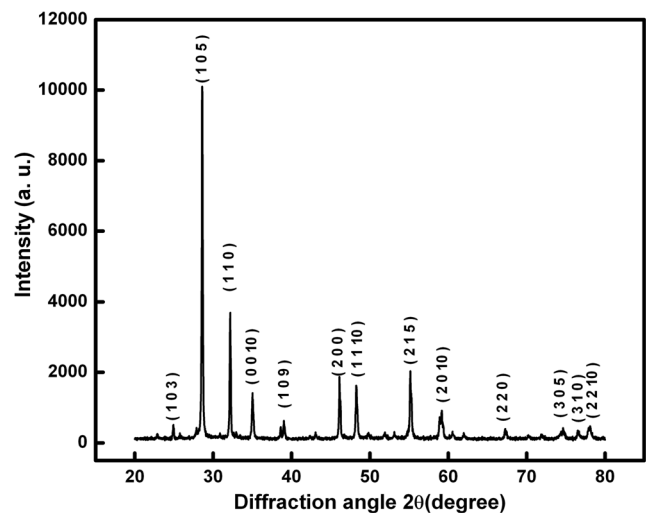


Fig. 1 XRD of $\text{BaBi}_2\text{Nb}_2\text{O}_9$

investigated the structure of $\text{BaBi}_2\text{Nb}_2\text{O}_9$ and found a and c value as 3.9398 \AA and 25.647 \AA respectively [11]. Thus, the values of the lattice parameters obtained are very much similar to the earlier reported one. The grain growth and the microstructure of $\text{BaBi}_2\text{Nb}_2\text{O}_9$ ceramics have been observed from the scanning electron microscopy (SEM) images shown in Fig 2(a). From the SEM micrograph, it is clear that the grain size is nearly uniform and the crystalline grain size varies in between 2 and $2.5 \mu\text{m}$. It also represents that the microstructure of the sample is dense, and have less number of scattered pores. Figure 2(b) shows Energy Dispersive Spectroscopy (EDS) spectra which confirms constituent elements (Ba, Bi, Nb and O) present in the sample.

3.2 Dielectric properties

3.2.1 Frequency dependence of dielectric properties

Figure 3(a) and (b) respectively shows the variation of dielectric constant (ϵ') and loss tangent ($\tan\delta$) with frequency ranging from 1 kHz to 1 MHz at different temperatures (i.e., at

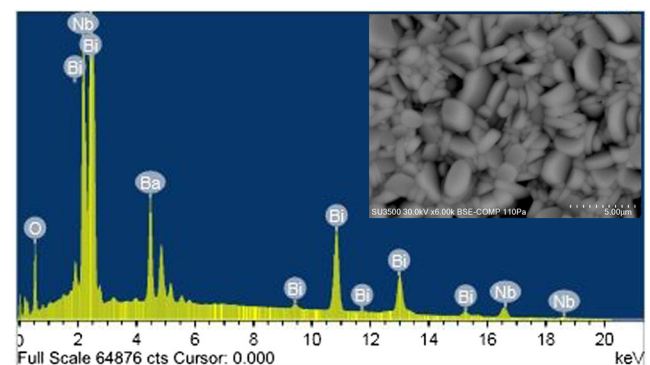


Fig. 2 SEM micrograph and EDS spectra of $\text{BaBi}_2\text{Nb}_2\text{O}_9$

100 °C, 200 °C, 300 °C, 400 °C, 500 °C). The variation of dielectric constant with frequency at room temperature is shown in Fig. 3(a) (inset). Both the dielectric constant and loss tangent value of the material decreases with increase in frequency and becomes constant at higher frequency range which is normal to many of the dielectric/ ferroelectric materials. The dielectric dispersion clearly appears at low temperatures and extends to the microwave region. A less pronounced dispersion of dielectric permittivity can be seen even at low temperatures. The value of dielectric constant at lower frequency range is higher because of various polarization effects in the sample. The dielectric permittivity at low temperatures behaves nearly linearly as it should be for relaxors [13, 14]. At low frequency, higher value of dielectric loss tangent is obtained due to the higher resistance offered by the grain boundaries as more energy is required for the motion of charge carriers. Similarly, at high frequency, low resistance is offered by grains, resulting in lower value of dielectric loss [15].

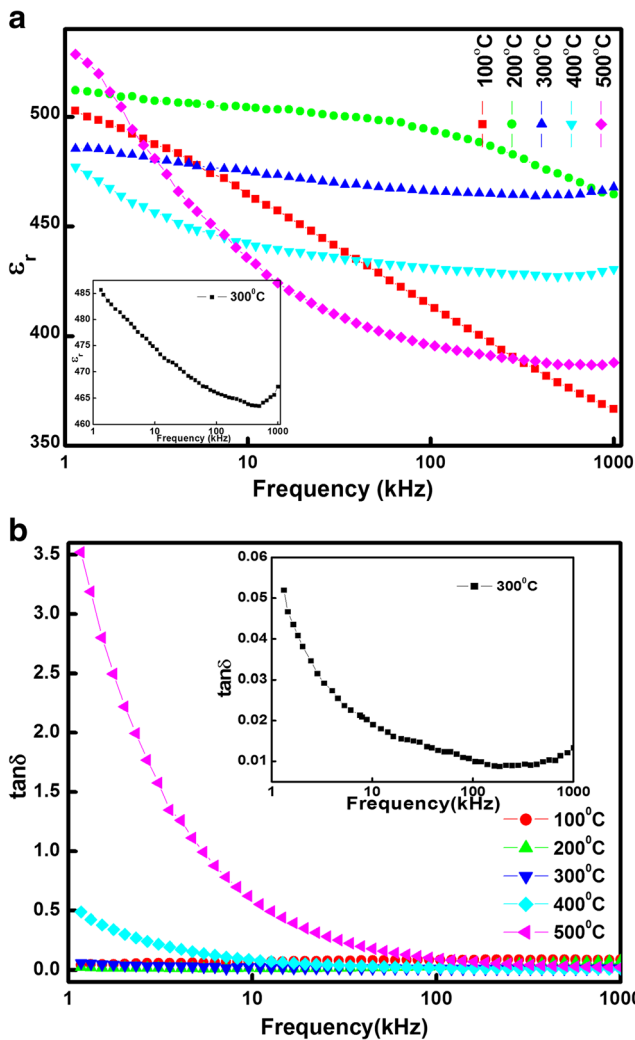


Fig. 3 Variation of (a) relative permittivity and (b) dielectric loss with frequency of BaBi₂Nb₂O₉ at varying temperatures

3.2.2 Temperature dependence of relative permittivity and tangent loss

Figure 4(a) and (b) represent the variation of the dielectric constant and loss factor with temperature (ranging from 25 °C- 500 °C) at several frequencies (50 kHz, 100 kHz, 300 kHz, 500 kHz, 700 kHz, 1 MHz) for BaBi₂Nb₂O₉. At 100 kHz, the dielectric constant increases rapidly with temperature and then reaches a maximum at 214.02 °C and then decreases gradually. Considering all the frequencies as shown in the Fig. 4(a), it could be observed that the maximum value of dielectric constant (ϵ_{max}) decreases with the increase of frequency and its corresponding temperatures i.e., the T_m value shifts up to higher temperatures, showing the relaxor mechanism and a phase transition from ferroelectric to paraelectric. This may be attributed to the reduced polarizability of the host ions and weak interaction between the dipole

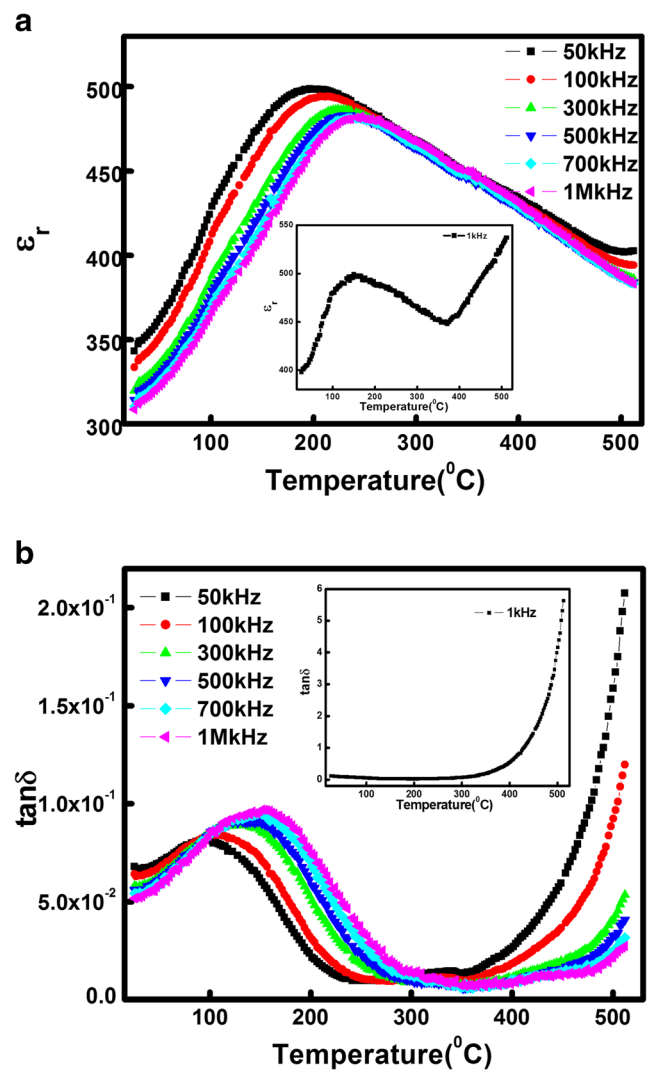


Fig. 4 Variation of (a) relative permittivity and (b) dielectric loss with temperature of BaBi₂Nb₂O₉ at different frequencies

moments in the layered structure. The reduction of dielectric constant at T_{max} with frequency are the typical features of a thermally activated Debye relaxation in the frequency space. Such Debye like anomaly is observed in the cubic phase of BaTiO₃ and PbTiO₃ [16]. Figure 4(b) which shows the temperature dependent loss of tangent (tanδ) increases with the temperature and reaches to maximum values at 93.81 °C, 101.022 °C, 134.755 °C, 149.42 °C and 151.86 °C for frequencies 50 kHz, 100 kHz, 300 kHz, 500 kHz and 1 MHz respectively, further the loss tangent increases again which may be due to the enhancement of conductivity (higher concentration of charge carriers at high temperature) or reduction in the ferroelectric domain wall contribution [17, 18].

Figure 5 shows the plot of $\ln(\nu/\nu_0)^{-1}$ versus T_m , where the solid line is the fitted line using the equation for linear fitting is: $T_m = T_f - \frac{E_a}{K_B} \cdot \left[\ln\left(\frac{E_a}{K_B}\right) \right]^{-1}$. In this equation, T_f is the static freezing temperature, where the spectrum of the relaxation times is expected to infinitely broaden, E_a is the activation energy, ν_0 is the Debye frequency which has a meaning of the inverse minimum relaxation time, and T_m is the temperature of the permittivity maximum. Using the above equation, it is seen that the linear curve fitting is in good agreement with reasonable standard deviations of the fitting parameters, and results in an activation energy of 0.357 eV, a pre-exponential factor (Debye frequency) of 1.5×10^{12} Hz, and a static freezing temperature of (226 ± 14) K. The observed good fit of the Vogel–Fulcher relation [19, 20] to the experimental data confirm the relaxor nature of the BBN ceramics.

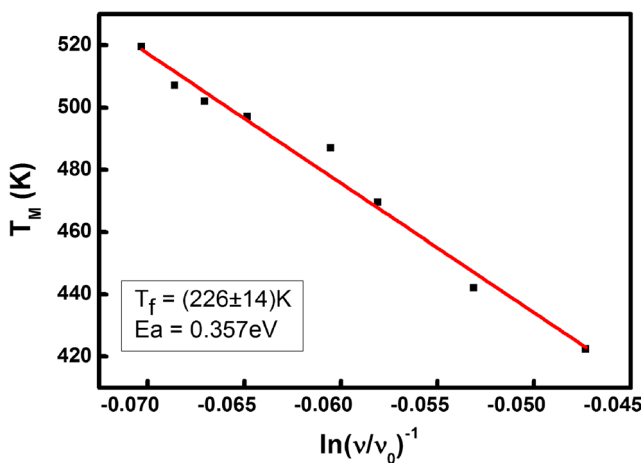


Fig. 5 Temperature of dielectric maximum as a function of measured frequencies of BaBi₂Nb₂O₉ ceramic

3.3 Ac conductivity analysis

The conductivity analysis provides the information about the domain structure and its motion, as well as the nature of charge carriers present in the system. Study of the mechanism of the formation of different conducting species in the sample is required to understand the effect of bulk conductivity on the dielectric, ferroelectric properties and fatigue resistance. The thermally activated conduction mechanisms of the materials classified into three categories as follows:

- (1) arises due to the formation of singly ionized and/ doubly ionized oxygen vacancy. The electrons liberated during this process can be captured by the ions in the given sample, and hence it will promote the electronic hopping between the states to trigger the temperature and frequency dependent electronic conductivity. Due to the creation of oxygen vacancies and combining the same with the ions in the material, there is also a possibility of formation of dipoles which will further affect the dielectric relaxation in the system [21]. According to Skanavi et al. [22] and Neirman et al. [23], oxygen vacancy is created by the loss of oxygen from the crystal lattice during sintering at higher temperature in air (low oxygen pressure) according to $O_{ox} \leftrightarrow V_{ox} + (\frac{1}{2}) O_2$, where V_{ox} is the oxygen vacancy.
- (2) formation of small polarons in the crystal can takes place by the interaction of electrons with the polar modes that is responsible for the conduction process in the transition region of ferro- to paraelectric [24].
- (3) at high temperature region, the occurrence of an intrinsic and a typical conduction mechanism can appear in ferroelectric materials [25].

3.3.1 Temperature dependence of ac conductivity

The ac conductivity of the material is calculated from the measured dielectric parameters by using a relation $\sigma_{ac} = \omega \epsilon_0 \epsilon_r \tan \delta$, where ω is the angular frequency, ϵ_0 is the permittivity in free space, and $\tan \delta$ is the tangent loss. The variation of σ_{ac} with $1000/T$ at different frequencies is shown in Fig. 6. A linear variation of σ_{ac} over a wide temperature range supports the existence of thermally activated transport properties of the materials that obey the Arrhenius equation:

$\sigma_{ac} = \sigma_0 \exp(-E_a/k_B T)$ (where σ_0 is the pre-exponential factor, E_a is the activation energy and K_B is the Boltzmann constant). It was observed from the graph that the conductivity increases with increase in temperature, and shows negative temperature coefficient of resistance (NTCR) behavior. The calculated value of E_a at 1 kHz, 100 kHz and 1 MHz in high temperature range (i.e., 280 °C–500 °C) was found to be

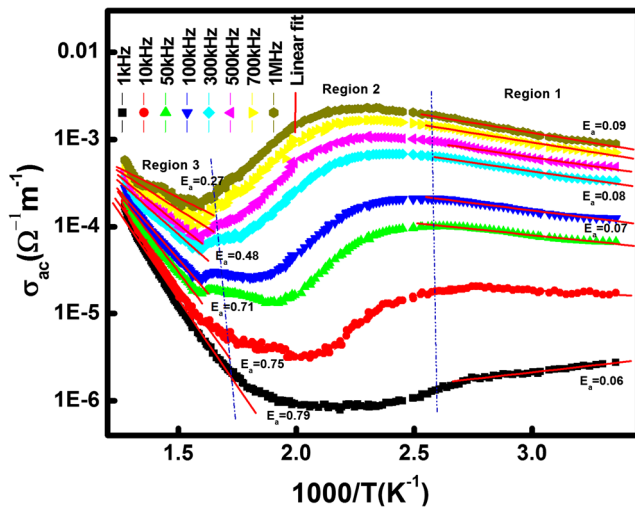


Fig. 6 Variation of ac conductivity with inverse temperature of $\text{BaBi}_2\text{Nb}_2\text{O}_9$ at different frequencies

0.79 eV, 0.62 eV and 0.27 eV and in low temperature range (i.e. 125 °C–25 °C), it was found to have values 0.06 eV, 0.07 eV, 0.09 eV respectively. The change in the slope in the graph at different temperature regime suggests that the conduction mechanism changes from one region to another [26]. In the lower frequency region (i.e., in Region 1), the ac conductivity varies independently with temperature for all the studied frequencies. The lower value of the activation energy (0.06 eV–0.09 eV) obtained at low temperatures (Region 1) is for the hopping charge mechanisms and it is associated mainly with the creation of large number of space charge carriers in oxidation–reduction process [27]. An anomaly is observed in the vicinity of dielectric maximum temperature (T_m). This shifts towards the higher temperatures with increase in frequency. In the higher temperature region (Region 3), the conductivity varies exponentially with temperature but very weakly dependent on frequency and ultimately all the curves are merged with a constant slope. This frequency independent behavior is attributed to the contribution from dc conduction [28]. The activation energy in this region varies from 0.79 to 0.27, which is attributed to the oxygen ion hopping. The increase in conductivity at higher temperature side is merely responsible for an increased loss of tangent, which was observed in $\tan\delta$ vs. temperature plot as shown in Fig. 4(b).

3.3.2 Frequency dependence of ac conductivity

Figure 7 shows the variation of ac conductivity over a broad range of frequency (1 kHz–1 MHz) at different temperatures. Generally, the conductivity consists of two parts, a frequency independent dc conductivity part and a highly dispersive ac conductivity part and this type of phenomenon can be explained by Jonscher's power law [29], given by the equation.

$\sigma_t = \sigma_{dc} + A\omega^n$ where, σ_t is the total conductivity, σ_{dc} is the dc conductivity, A is a temperature dependent constant which

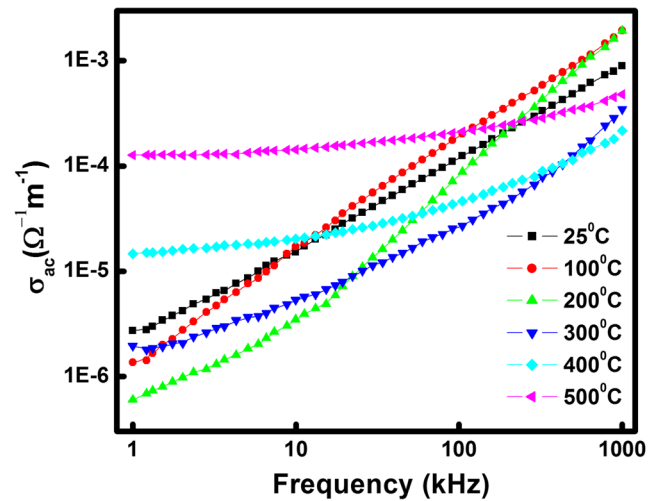


Fig. 7 Variation of AC conductivity as a function of frequency at different temperatures of $\text{BaBi}_2\text{Nb}_2\text{O}_9$

also depend on the intrinsic material property and n is the power law exponent. The exponent n represents the degree of interaction between mobile ions with the lattice around them. The pre factor A determines the strength of polarizability. A typical fit of Jonscher's power law equation to the experimental data is shown in Fig. 8. The dc value obtained from power law fitting at selected temperatures are given in Table 1.

3.4 Impedance studies

3.4.1 Variation of complex impedance parameters with frequency

Impedance spectroscopy is a vital and widely used tool for the electrical characterization of materials [30–32] over a wide range of frequency and temperature. It is necessary to understand the contribution of grain, grain boundary and interface

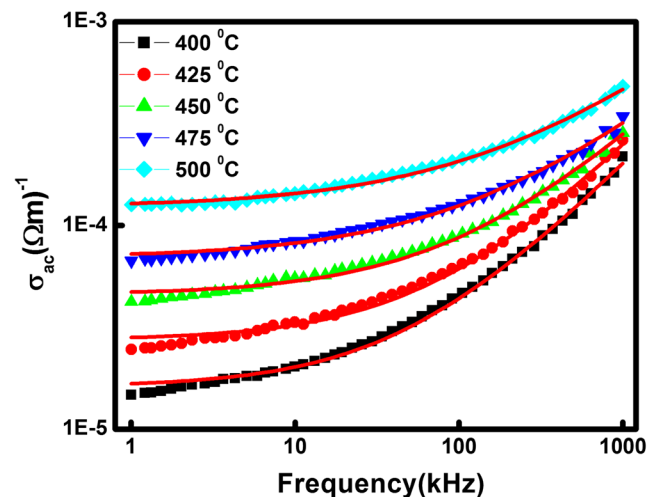


Fig. 8 Experimental and theoretical fit for AC conductivity as a function of frequency

Table 1 dc value obtained from power law fitting at selected temperatures

Temperature(°C)	$\sigma_{dc}(\text{ohm}^{-1} \text{ cm}^{-1})$
400 °C	0.00002
425 °C	0.00003
450 °C	0.00005
475 °C	0.00007
500 °C	0.00012

effects, which greatly influence on the electrical properties. The electrical response of the material can be understood by the basic formalisms of the complex permittivity (ϵ^*), complex impedance (Z^*), complex admittance (Y^*), complex electric modulus (M^*) and dielectric loss or dissipation factor ($\tan\delta$), which are interrelated to each other [33]. These relations offer a wide scope for a structure-property analysis of the various parameters under different conditions (temperature or frequency) through graphs. The real (Z') and imaginary (Z'') of the complex impedance (Z^*) can be defined by the following equation [34]:

$$Z'' = \frac{\omega R}{1 + (\omega\tau)^2} \text{ and } Z' = \frac{R}{1 + (\omega\tau)^2}$$

where, $\tau = RC$ is the relaxation time, R and C are the measured resistance and capacitance, ω is the angular frequency of the electric field.

Figure 9 shows the frequency dependence of the real (Z') and imaginary (Z'') part of complex impedance at various temperatures starting from room temperature. With the increase in frequency, the values of Z' decreased up to a particular frequency depending on the temperature and all the curves merge to a single line at higher frequency side indicating the temperature independent mechanism and release of space charge. At lower frequency region the decreasing in Z' signifies NTCR (negative temperature coefficient of resistance) nature of the material [35]. The rate of decrease of Z' with frequency increases as temperature is increased. However, Z'' value increased rapidly with increase in frequency and attains saturation value after which its value remains constant with respect to frequency for almost all the temperatures. Figure 9 (inset) shows the variation of Z'' at higher temperature range (400 °C- 500 °C) which manifests the rise of Z'' with increase in frequency at all the temperatures and exhibits a maximum. The broadening of the peaks with increasing temperature suggests the deviation from the ideal Debye behavior [36] and presence of temperature dependent relaxation process in these materials [37]. The relaxation process may be due to the presence of non-homogeneous distribution of ion space charges participating in the screening process of the polar-regions [38]. The occurrence of the polar-regions and their interaction with free electron and ion space charges can be identified by thermally stimulated

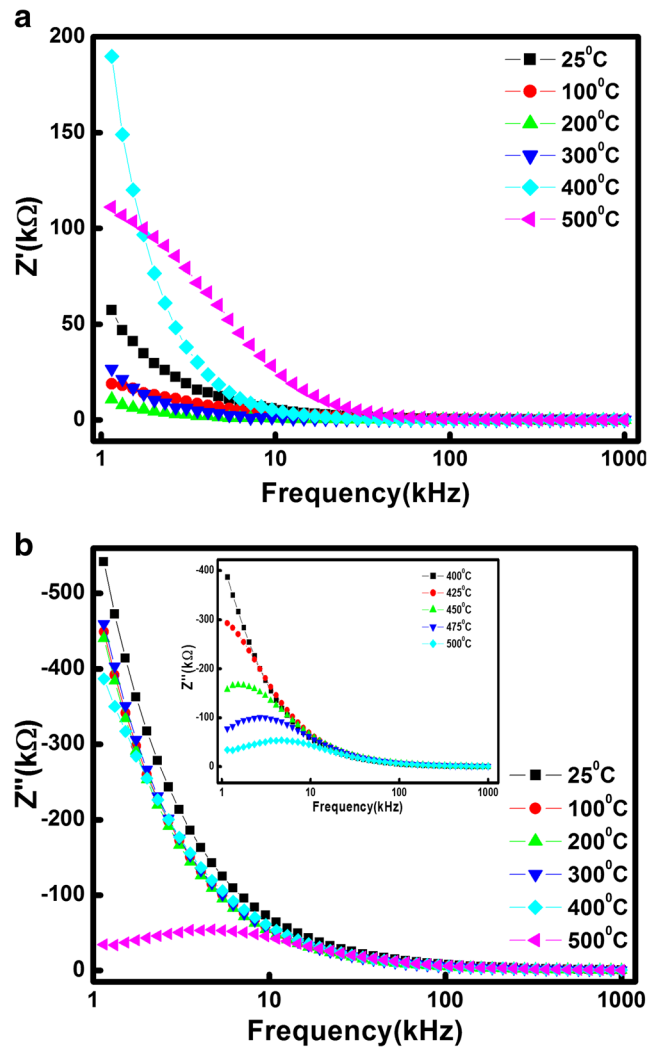


Fig. 9 Frequency dependence of real (a) and imaginary (b) part of the impedance at various temperature

depolarization current (TSDC) studies [39, 40]. Moreover, the shifting of Z'' peaks towards low frequency side with decrease in temperature indicates a decrease in relaxation in the system [41].

3.4.2 Niquist plot

The variation of Z' with Z'' at different temperatures are known as the Niquist plot (complex impedance plot) and also the cole-cole plot. Though by using impedance spectroscopy, we can extract information on electrical conduction process, by modeling the impedance experimental data with a proper equivalent circuit we can obtain much more information. Generally, the impedance data obtained from the experiment are fitted with the impedance of an equivalent circuit consists of ideal resistors and capacitors. In some cases, use of constant phase element (CPE) is needed to represent non-Debye type behavior. The CPEs describe the “power law” dependence of the impedance components on frequency. The CPE

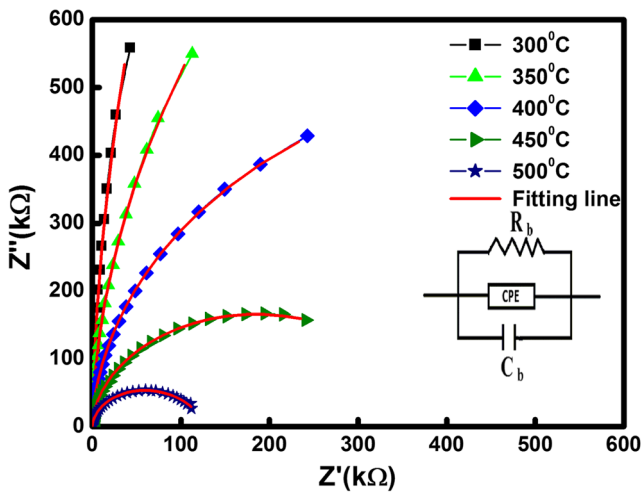


Fig. 10 Variation of Z' with Z'' of $\text{BaBi}_2\text{Nb}_2\text{O}_9$ at different Temperatures

impedance is given by $Z_{CPE} = [A_0(j\omega)^p]^{-1}$, where $A_0 = A / \cos(n\pi/2)$ and $j = \sqrt{-1}$. Here, A and p are the frequency-independent but temperature dependent parameters. The value of p lies between 0 and 1 ($p = 1$ for an ideal capacitor and $p = 0$ for an ideal resistor).

In complex impedance plot one, two or three semicircles or semicircular arcs are obtained depending on the behavior of the corresponding sample under study. In Nyquist plot, single semicircular arc represents the electrical response due to the interior of the grain. When double semicircles are assigned to the Nyquist plot, both grain and grain boundary effect is observed and the third one represents contribution of interface to electric conductivity. Generally, the center of these arcs is depressed and is below the real impedance axis implying departure from Debye type behavior. This non-ideal behavior can be correlated to grain orientation, grain boundary, stress-strain phenomena and atomic defect distribution respectively. The depression of the semicircle is considered further the evidence of polarization phenomena with a distribution of relaxation time. In ideal case, when the center of the semicircular arc is on the real impedance axis, then the system is said to follow Debye type behavior. Each semicircular arc can be explained by RC circuits [42, 43].

A representative graph of complex impedance spectra of $\text{BaBi}_2\text{Nb}_2\text{O}_9$ has been shown in Fig. 10. As shown in the graph, we obtain a single semicircular arc from the Nyquist

Table 2 Grain resistance (R_b), grain capacitance (C_g), quality factor (CPE) and n at selected temperatures

Temperature(°C)	R_b (Ω)	C_b (F)	CPE (Q)	n
300 °C	1.082×10^7	2.746×10^{-10}	8.849×10^{-11}	8.444×10^{-1}
350 °C	3.499×10^6	2.707×10^{-10}	4.428×10^{-10}	6.461×10^{-1}
400 °C	1.159×10^6	2.588×10^{-10}	1.409×10^{-9}	5.897×10^{-1}
450 °C	4.248×10^5	2.469×10^{-10}	1.878×10^{-8}	4.132×10^{-1}
500 °C	1.339×10^5	2.333×10^{-10}	2.687×10^{-8}	4.331×10^{-1}

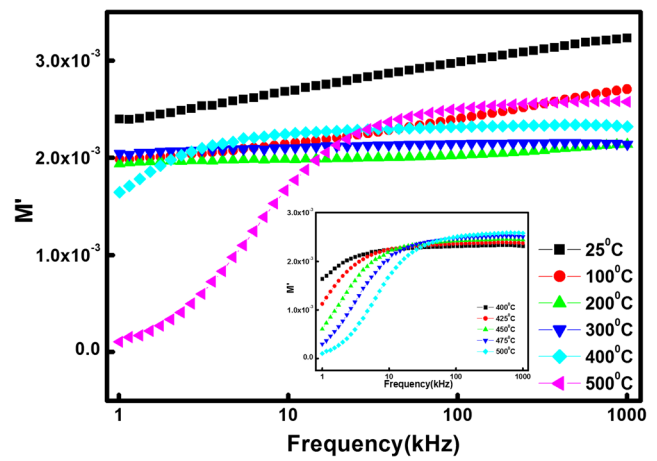


Fig. 11 Variation of M' with frequency at different temperatures

plot of the sample whose center is below the real impedance axis, implying the departure from Debye type behavior. According to the Debye’s model, a material having single relaxation time gives rise to an ideal semicircle centered on the real axis [44]. Occurrence of single semicircular arc represents that the electrical properties of the sample is due to grain(bulk). It also depicts the absence of electrode polarization and confinement of relaxation process to the bulk of the crystal. It also indicates that the intercept point on the real impedance axis shifts towards the origin, with the rise in temperature indicating the decrease in the resistive property of the material. The values of grain resistance (R_b), grain capacitance (C_g), quality factor (CPE) and n at selected temperatures have been provided in Table 2.

3.5 Modulus spectroscopy

The complex electric modulus spectroscopy analyses the electrical transport phenomenon and relaxation mechanism in the materials. Figure 11 shows the frequency dependence of real part of complex electric modulus (M') at some selected temperatures and the plots in the temperature range of 400 °C–500 °C are shown in the inset of Fig. 11. It is observed that in the lower temperature region, the value of M' increases slowly with increase in frequency, the value of M' increases slowly with the increase in temperature, while in the higher temperature region, M' has very low value at lower frequency but rises sharply

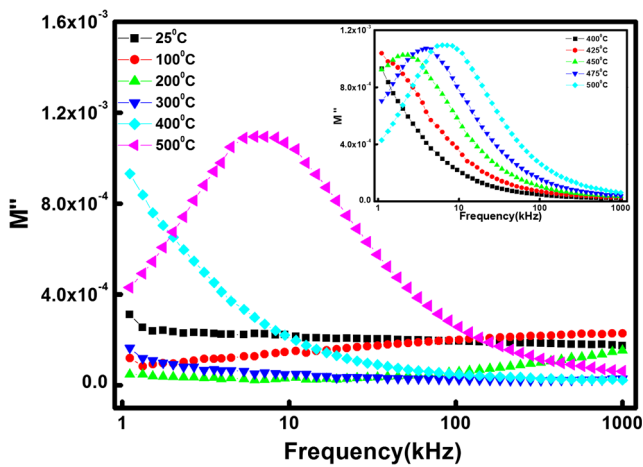


Fig. 12 Variation of M'' with frequency at different temperatures

with the increase in frequency tending to acquire a higher saturated value which increases with increase in temperature. It confirms the absence of an appreciable electrode polarization and is related to the frequency invariant electrical properties of the materials. Therefore, slow increase of M' at lower temperature and rapid increase of the same at higher temperatures with frequency indicates continuous dispersion on increasing frequency and it may be contributed to the conduction phenomena due to short range mobility of charge carriers. This confirms the elimination of electrode effect in the material and the lack of restoring force for the flow of charge under the influence of a steady electric field [45]. At higher temperatures, the dispersion region shifts towards higher frequency side supporting the long range mobility of charge carriers.

Figure 12 shows the variation of M'' with frequency, which clearly shows that, at lower temperatures (25 °C–300 °C), the value of M'' is nearly zero and it is almost

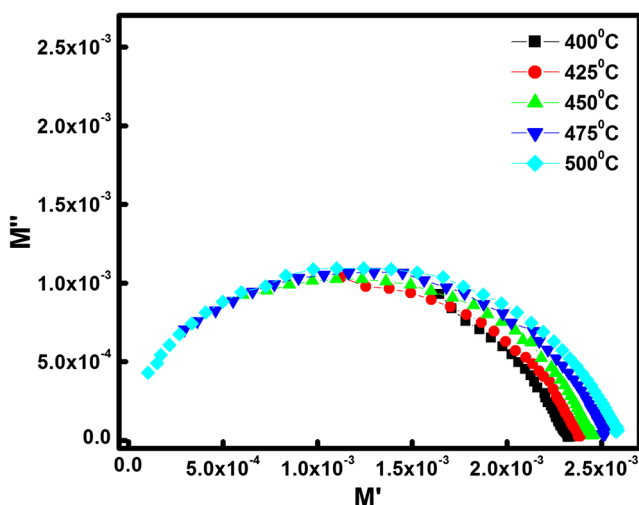


Fig. 13 Variation of M' with M'' at different temperatures

constant throughout the frequency range without any peak, but at higher temperatures i.e., from 400 °C to 500 °C (inset of Fig. 12), the peaks shift systematically towards higher frequencies with increase in temperature. Here, the peaks correspond to a relaxation process where the peak height is inversely proportional to the capacitance of the material. The peak shift shows the thermal activated nature of the relaxation time. The frequency region below the peak frequency determines the range where the charge carriers are mobile over long distances whereas above the peak, the carriers are confined to a potential well and are mobile over short distances [46].

In Fig. 13, a semicircular arc with a tendency to form two semicircular arcs indicates the presence of grain and grain boundary contribution at higher temperatures. The appearance of these semicircles with their centers lying below the real M' axis indicates the spread of relaxation with different time constants and manifests the presence of non-Debye type of relaxation in the material. From the graph, it is clear that with increase in temperature, the intercept of the complex modulus plots on real M' axis shifts towards the higher values of M' which indicates increase in capacitance of the samples as temperature increases. It supports the negative temperature coefficient of resistance (NTCR) type behavior of the material since bulk capacitance (C_b) is inversely proportional to the bulk resistance (R_b).

4 Conclusions

$BaBi_2Nb_2O_9$ has been successfully prepared via solid state process. The crystal structure of the compound is found to be tetragonal from XRD analysis. The surface morphology studies shows the formation of uniform grains over the entire surface of the sample. From dielectric studies, it is clear that the parameters are strongly temperature and frequency dependent. The studied samples showed typical relaxor behavior with strong dispersion of the dielectric parameters. The relaxor nature of the $BaBi_2Nb_2O_9$ ceramics was confirmed by the good fit of the Vogel–Fulcher relation to the experimental data. The impedance behavior of $BaBi_2Nb_2O_9$ ceramics was found to exhibit (1) bulk effects, (2) semiconducting nature (NTCR-type behavior), and (3) non-Debye type of relaxation phenomena. A linear variation of σ_{ac} over a wide temperature range supports the existence of thermally activated transport properties of the materials that obey the Arrhenius equation. The variation of ac conductivity with frequency obeys Jonscher’s universal power law. Complex modulus plots show the presence of both the grain and grain boundary effect in the material whereas impedance analysis indicates the grain effect only.

References

- C.A.P. de Arauzo, J.F. Scott, *Science* **246**, 1400 (1989)
- A.I. Kingon, *Current opinion in solid state and materials science*, Elsevier, 1999, p. 39
- E.C. Subbarao, *J. Am. Ceram. Soc.* **45**(4), 166–169 (1962)
- E.C. Subbarao, *J. Phys. Chem. Solids* **23**(6), 665–676 (1962)
- A.L. Kholkin, M. Avdeev, M.E.V. Costa, J.L. Bapista, S.N. Dorogovtsev, *Appl. Phys. Lett.* **79**(5), 662–664 (2001)
- C.-H. Lu, C.-Y. Wen, *Mater. Lett.* **38**(4), 278–282 (1999)
- Y. Xu, *Ferroelectric materials and their applications* (Elsevier, Amsterdam, 1991)
- L.E. Cross, *Ferroelectrics* **151**(1), 305–320 (1994)
- Y. Shimakawa, Y. Kubo, Y. Nakagawa, S. Goto, T. Kamiyama, H. Asano, F. Izumi, *Phys. Rev. B* **61**(10), 6559–6564 (2000)
- S.M. Blake, M.J. Falconer, M. McCreedy, P. Lightfoot, *J. Mater. Chem.* **7**(8), 1609–1613 (1997)
- B.J. Ismunandar, Kennedy, *J. Mater. Chem.* **9**, 541 (1999)
- G.A. Smolenskii, V.A. Isupov, A.I. Agranovskaya, *Sov. Phys. Solid State* **3**, 651 (1961)
- P. Keburis, J. Banys, A. Brilingas, J. Prapuolenis, A. Kholkin, M.E.V. Costa, *Ferroelectrics* **353**(1), 149–153 (2007)
- V.V. Shvartsman, M.E. Costa, M. Avdeev, A.L. Kholkin, *Ferroelectrics* **296**(1), 187–197 (2003)
- M. Sahni, N. Kumar, S. Singh, A. Jha, S. Chaubey, M. Kumar, M.K. Sharma, *J. Mater. Sci. Mater. Electron.* **25**, 2199 (2014)
- O. Bidault, P. Goux, M. Kchikech, M. Belkaoui, M. Maglione, *Phys. Rev. B* **49**(12), 7868–7873 (1994)
- P. Khatri, B. Behera, R.P.N. Choudhary, Structural and impedance properties of $\text{Ca}_3\text{Nb}_2\text{O}_8$ ceramics. *J. Phys. Chem. Solids* **70**(2), 385–389 (2009)
- R. Ramaraghavulu, S. Buddhudu, *Ferroelectrics* **460**, 57–67 (2014) 1563–5112
- H. Vogel, *Phys. Z.* **22**, 645–646 (1921)
- G. Fulcher, *J. Amer. Ceram. Soc.* **8**(6), 339–355 (1925)
- D.K. Pradhan, R.N.P. Choudhary, C. Rinaldi, R.S. Katiyar, *J. Appl. Phys.* **106**(2), 024102–024110 (2009)
- G.I. Skanavi, E.N. Matveeva, *Sov. Phys. JETP* **3**, 905 (1957)
- I. Burn, S. Neirman, *J. Mater. Sci.* **17**(12), 3510–3524 (1982)
- K.C. Kao, *Dielectric phenomena in solids* (Elsevier Academic Press, London, UK, 2004)
- O. Bidault, P. Goux, M. Kchikech, M. Belkaoui, M. Maglione, *Phys. Rev. B* **49**(12), 7868–7873 (1994)
- S. Sinha, S.K. Chatterjee, J. Ghosh, A.K. Meikap, *J. Phys. D. Appl. Phys.* **47**(27), 275301 (2014)
- N. Kumar, S.K. Patri, R.N.P. Choudhary, *J. Alloys Compd.* **615**, 456–460 (2014)
- C. Karthik, K.B.R. Varma, *J. Phys. Chem. Solids* **67**(12), 2437–2441 (2006)
- A.K. Jonscher, *Dielectric relaxation in solids* (Chelsea Dielectric Press, London, 1983)
- S. Lanfredi, A.C.M. Rodrigues, *J. Appl. Phys.* **86**(4), 2215–2219 (1999)
- D.C. Sinclair, A.R. West, *J. Appl. Phys.* **66**(8), 3850–3856 (1989)
- T.S. Irvine, D.C. Sinclair, A.R. West, *Adv. Mater.* **2**(3), 132–138 (1990)
- I.M. Hodge, M.D. Ingram, A.R. West, *J. Electroanal. Chem.* **74**(2), 125–143 (1976)
- M. Azizar Rahman, A.K.M. Akther Hossain, *Phys. Scr.* **89**(11), 115811 (2014)
- A. Rouahi, A. Kahouli, F. Challali, M.P. Besland, C. Vallee, B. Yangui, S. Salimy, A. Goullet, A. Sylvestre, *J. Phys. D. Appl. Phys.* **46**(6), 065308 (2013)
- Y.-M. Li, W. Chen, J. Zhou, Q. Xu, X.-Y. Gu, R.-H. Liao, *Physica B* **365**(1–4), 76–81 (2005)
- A.K. Jonscher, The universe dielectric response. *Nature* **267**(5613), 673–679 (1977)
- J. Ha'nderek, Z. Ujma, C. Carabatos-Nedelec, G.E. Kugel, D. Dmytr'ow, I. El-Harrad, *J. Appl. Phys.* **73**, 367–373 (1993)
- Z. Ujma, M. Adamczyk, J. Ha'nderek, *J. Europ. Ceram. Soc.* **18**(14), 2201–2008 (1998)
- P. Braunlich, *Topics in Appl. Phys.* **37**, 35–91 (1979)
- M. Adamczyk, L. Kozeilski, A.N.D.M. Pilch, *Ferroelectrics* **417**(1), 1–8 (2011)
- M.A. Ahmed, S.F. Mansour, M.A. Abdo, *Phys. Scr.* **86**(2), 025705 (2012)
- S. Sahoo, P.K. Mahapatra, R.N.P. Choudhary, M.L. Nandagoswamy, *J. Mater. Sci. Mater. Electron.* **26**, 6572–6584 (2015)
- A.K. Jonscher, Dielectricrelaxationinsolids, *Nature (London)* **267** (1977), 673–679
- P.B. Macedo, C.T. Moynihan, R. Bose, *Phys. Chem. Glasses* **13** (1972)
- D.K. Mahato, A. Dutta, T.P. Sinha, *Phys. B* **406**(13), 2703–2708 (2011)